Let's Talk Trash: The Enzymatic Degradation of Polyethylene Teraphalate Through Genetically Engineered *Escherichia coli*

Aaron Berg (berga7, 400509948)

Aaron Zhao (zhaoa38, 400496412)

Laura No (noj2, 400498663)

Liam Berry (berryl7, 400496344)

Anoojen Vakeesan (vakeesaa, 40052911)

IBEHS 2P03

Health Solutions Design Projects II: Introduction to Genetic Engineering

L01

Date submitted: April 8, 2025

Instructor:

Dr. Vincent Leung

Abstract

This article proposes the use of synthetic biology to develop a more complete breakdown of polyethylene terephthalate (PET). While current solutions focus on the breakdown of PET into its subunits ethylene glycol (EG) and terephthalic acid (TPA), the proposed method considers the toxicity of EG and breaks it down into safe derivatives. The circuit detects PET from byproducts released during natural PET degradation and produces the enzymes to break PET into EG and TPA and degrade EG into malate. The circuit was modelled using Simbiology and a Golden Gate BioBrick assembly will be used to construct it. Preliminary results from the model indicate circuit efficacy toward sufficiently increasing the rate of PET degradation, with some indications of inefficiencies in the downstream functionality of the circuit towards EG degradation.

Table of Contents

Table of Contents Graphic

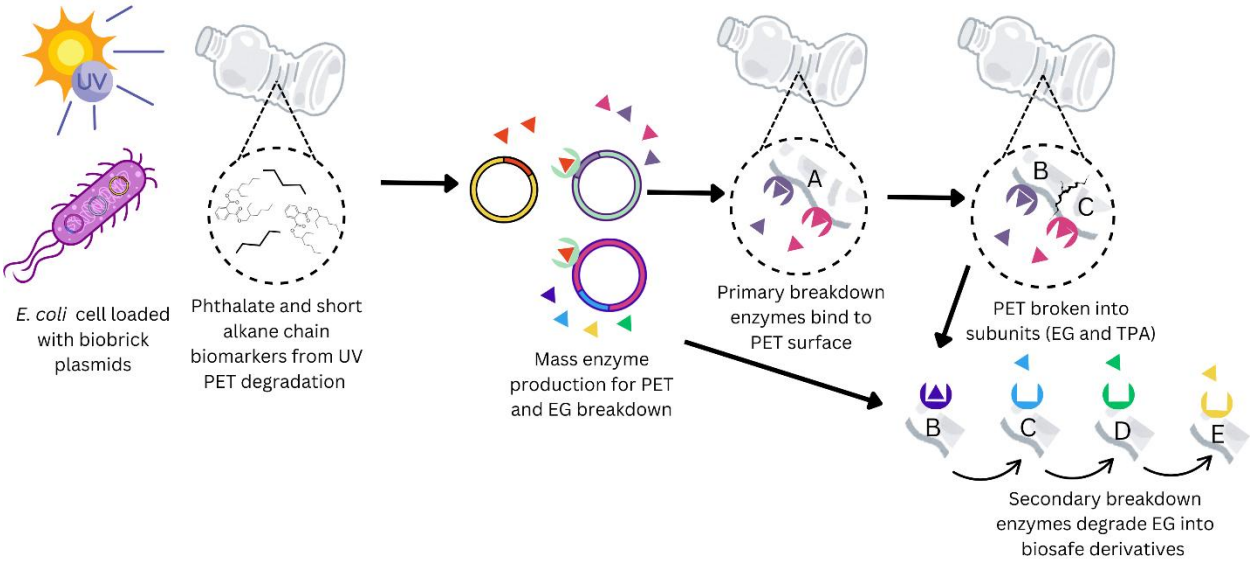

Figure 1: The proposed solution for complete PET breakdown. The plasmids within the E. coli cells detect the presence of PET through byproducts of its natural degradation. This creates a chain of enzymes that are mass produced to break PET down into EG and TPA, then further breakdown EG into malate and coenzyme A (CoA).

Introduction

PET is one of the most widely used plastics due to its durability, transparency, lightweight properties, and cost effectiveness, however its widespread use has led to significant environmental concerns [1]. Between 2015 and 2020, approximately 6.3 billion tons of plastic waste were generated, with 79% either discarded or ending up in landfills [2].

Plastic pollution poses severe risks, not only to biodiversity, but also to human health. PET is particularly problematic due to its slow degradation rate, leading to long-term accumulation and damage to ecosystems [3]. Microplastic particles are also highly linked to various health issues, including reproductive problems, developmental delays, and hormonal imbalances [4].

Some physical characteristics of PET make it resistant to degradation, however recent research has introduced promising solutions [5]. In particular, the discovery of *Ideonella sakaiensis,* a bacterium capable of breaking down PET using enzymes, has sparked interest in microbial plastic degradation, but efficiency remains low [6]. To address these limitations, researchers are leveraging genetic engineering to enhance PET degradation. Engineered strains of *Escherichia coli* (*E. coli)* have been modified to produced PET degrading enzymes with increased efficiency [7]. Moreover, careful management of the byproducts and optimization of degradation pathways remain critical to improve the overall effectiveness.

In this study, the issue of plastic pollution is examined, with a focus on PET and its implications. The proposed circuit leverages genetically engineered *E. coli* to produce enzymes that degrade both PET and its toxic byproducts.

The results highlight the efficiency of enzymatic PET degradation and identify limitations such as metabolic bottlenecks and biomarker reliance. By integrating synthetic biology, this research contributes to development of innovative strategies for addressing plastic waste.

Materials and Methods

The construction of the polyethylene-degrading genetic circuit leverages a modular design comprising three functionally distinct components: two logic AND gates for signal integration, a PET degradation module encoding enzymes for breaking down polyethylene terephthalate, and an EG metabolism module to break down EG into non-toxic byproducts (*Table 1*). Specifically, the first logic AND gate constitutively produces peroxisome proliferator-activated receptor alpha (PPAR-α) and human retinoid X receptor alpha (RXR-alpha), both of which complex together to form a PPAR-RXR complex in the presence of arabinose. The second consecutive AND gate is expressed in the presence of a phthalate-based plasticizer commonly found in plastics, consequently producing functional T7. The T7 moves downstream in the circuit to produce both the PET-degradative enzymes and the ethylene glycol-degrative enzymes simultaneously.

Each module is independently assembled using a one-pot Golden Gate assembly reaction with BsaI-HFv2 and T4 DNA ligase. BsaI-HFv2 works by cutting DNA at specific recognition sites to assemble multiple DNA fragments together (*Table 2*). This method was chosen for its ability to generate scarless, directional ligation through custom 4-base overhangs that are carefully designed to ensure that each fragment is inserted in the correct orientation and order [8]. In particular, the downstream sequences (overhangs) are selected to be complementary only to the intended upstream sequence of the adjacent fragment, thereby enforcing the correct fragment order. Moreover, the BsaI cut site is absent within the coding sequences of our parts, ensuring compatibility isn't an issue [9].

To avoid incompatibility during transformation, DNA fragments—whether synthesized by IDT or obtained from iGEM/AddGene—are individually cloned into distinct plasmid backbones. Specifically, the two AND gates are inserted into separate plasmids: one in pSB1A3 (ColE1 origin, ampicillin resistance) and the other in pSB3K3 (p15A origin, kanamycin resistance). The PET degradation module is cloned into pSB4C5 (pSC101 origin, chloramphenicol resistance), while the EG metabolism module is now inserted into a plasmid with the pBBR1 origin (gentamicin resistance), ensuring that the two modules utilize different replication origins [10].

For DNA assembly, fragments are prepared by PCR-amplifying them with a high-fidelity enzyme, using materials outlined in *Table 3* to minimize errors such as accidental insertions and deletions, and to incorporate the designed BsaI sites and complementary 4-base overhangs [11]. These PCR products are then purified using a PCR purification kit (e.g QIAquick). Next, nucleic acid and protein concentrations are measured with a Qubit fluorometer so they can be mixed at the

correct ratios for ligation. A thermocycler protocol then runs for 25 cycles that alternates between 37°C to maximize digestion and 16°C to favor ligation. The assembled plasmids are then introduced into competent *E. coli* via electroporation (see *Table 5*); the cells recover in nutrient-rich media and are plated on agar with the proper antibiotics.

To verify construct integrity, individual transformant colonies are picked and grown in overnight cultures, a plasmid miniprep is performed to obtain purified DNA, and a PCR is carried out using primers flanking the inserted regions (*Table 4*).

To validate the circuit's efficacy in degrading polyethylene, an in vitro experiment will be conducted using four reactions in sealed glass vials containing M9 minimal medium, polyethylene fragments, and activators (L-arabinose and hexadecane) to enhance the reaction without introducing toxicity [12][13][14][15][16][17]. All vials will maintain identical conditions to control for variables such as pH and temperature. The test vial will include plasmid-bearing *E. coli*, the negative control will have plasmid-free *E. coli*, the blank will contain only medium, and the positive control will include purified enzymes produced by the circuit (SbPETase, MHETase, glycolaldehyde reductase (GR), glycolaldehyde dehydrogenase (GDH), glycolate oxidase (GO), malate synthase (MS)). Vials will be prepared aseptically in a biological safety cabinet, sealed (oxygen is not a concern since *E. coli* can grow anaerobically), and incubated for 48 hours at 37°C with agitation [18][19]. Sampling will occur every 12 hours to measure pH via spectrophotometry and pyruvate using a Cayman Chemical assay [20][21]. After incubation, dissolved CO_2 will be quantified by gas chromatography [21]. The expected outcome is that the test and positive control vials will exhibit increased CO_2 and pyruvate levels but a lower pH, confirming enzyme activity and polyethylene degradation. In contrast, the blank and negative controls are expected to remain relatively unchanged, establishing a baseline for natural degradation [21]. Data collected over time will enable the creation of a kinetic profile, allowing researchers to assess how effectively the engineered circuit accelerates degradation relative to natural processes, ultimately demonstrating the circuit's intended function [21][22]. The efficacy test can be seen in *Figure 8* for reference purposes.

Results and Discussion

Using MATLAB Symbiology, the biological circuit was constructed for simulation purposes. The SBOL diagram can be seen in *Figure 7* and the complete simulation can be seen in *Figure 9* for reference. For ease of discussion, *Figures 10, 11,* and *12* show magnified views of the T7 synthesis, PET enzymatic degradation, and EG enzymatic degradation cascade subcircuits respectively.

Formation of PPAR-RXR Complex for AND Gate Detection Mechanism

As seen in *Figure 2b,* the RXR-alpha gene has a linear relationship with the heterodimer molarity. From *Figure 2a* and *Figure 2c,* there appears to be logarithmic behaviour of the molarity of both PPAR-alpha and phthalate over the simulation.

The results from *Figure 2* demonstrate the functionality of the circuit's AND gate logic to complex PPAR-alpha and RXR-alpha into a functional heterodimer activated by the ligation binding of phthalate (see *Figure 10*) [23]. The proportionality of the heterodimer molarity with that of RXR-alpha suggests that RXR-alpha is a limiting reactant of the complexation rate and is thus the rate determining protein. This is confirmed by the near instant halt of PPAR-alpha which is expected as it follows standard enzyme kinetics.

The phthalate's logarithmic behaviour is also expected - considering that the phthalate would be bound the PET as an additive and, as PET is degraded, phthalate groups would be released. Furthermore, as PET became less abundant, less phthalate would become available, limiting the rate of its growth.

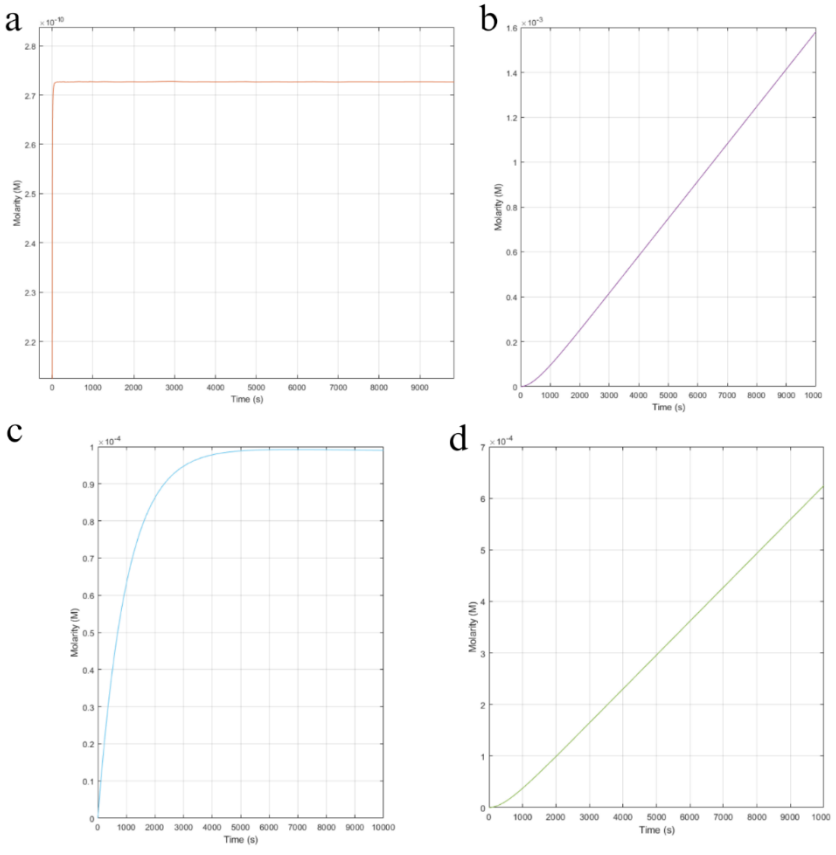

Figure 2: Molarity of PPAR-alpha over time (a), molarity of RXR-alpha over time (b), molarity of phthalate over time (c), and molarity of PPAR-RXR heterodimer complex over time (d), respectively. All figures ran with initial concentration of arabinose as 1e-10 M and an initial molarity of PET as 0.1 mM

Production of Functional T7 AND Gate Mechanism

T7 polymerase is used as the intermediary greenlight to produce the circuit's degradative enzymes. The production of T7 relies on the production of PPAR-RXR (see *Figure 2d*) and the presence of alkanes (see *Figure 3a)*. As seen in *Figure 3c*, once alkanes have induced the respective BioBrick, SupD-tRNA is produced. The production of SupD-tRNA shows a rate that initially increases exponentially but quickly degrades into what appears to be an upper bound asymptote. The PAR-RXR activated complex binds to a peroxisome proliferated-response element (PPRE) DNA sequence upstream of a minimal promoter causing the upregulation of T7 polymerase with an amber mutation (T7ptag). Seen in *Figure 3d*, the concentration of T7ptag shows a similar reaction rate profile to SupD-tRNA with less exaggerated asymptotic behaviour. From the presence of SupD-tRNA, T7 can be produced (see *Figure 3b*) instead of T7ptag. The rate of T7 production appears to be minimally exponential and aligns more with a linear rate of increase at a magnitude of 10^{-9} in the 10,000 second run time.

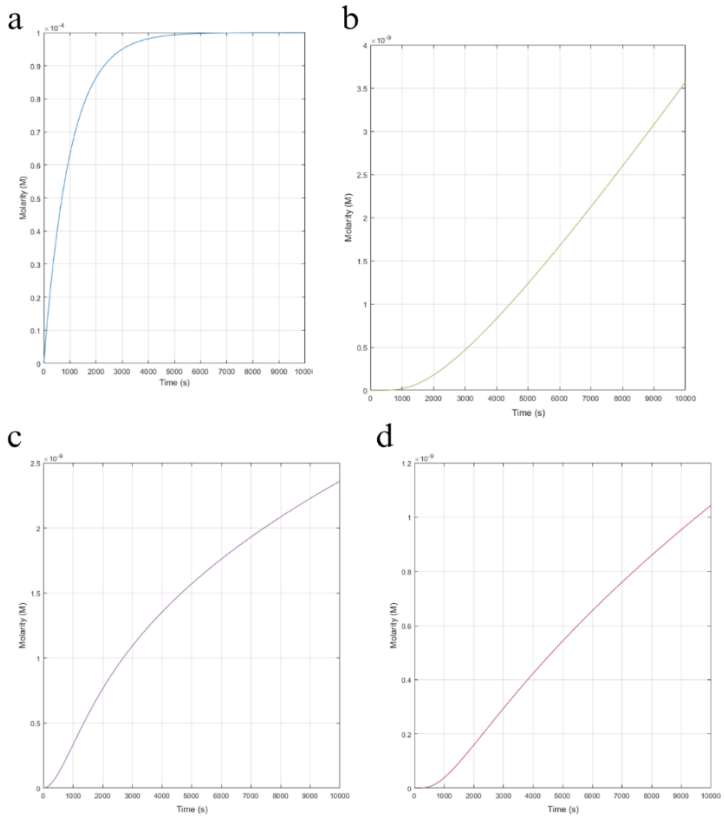

Figure 3: Alkane molarity over time (a), T7 molarity over time (b), SupD-tRNA molarity over time (c) (note that this is an assumption for the functionality of the simulation), and molarity of T7ptag over time (d).

Primary PET Degradation

Once T7 is deployed it invokes the primary PET degradation BioBrick. This produces PETase and MHETase, responsible for the breakdown of PET into EG and TPA (see *Figure 11*) [24]. As seen in *Figure 4a* and *Figure 4b*, both TPA and EG have the same behaviour of an exponential increase followed by logarithmic plateauing. *Figures 4c* and *4d* show similar exponential behaviour in the reaction profiles for sbPETase and MHETase whereas PET degrades exponentially (see *Figure 4e)*.

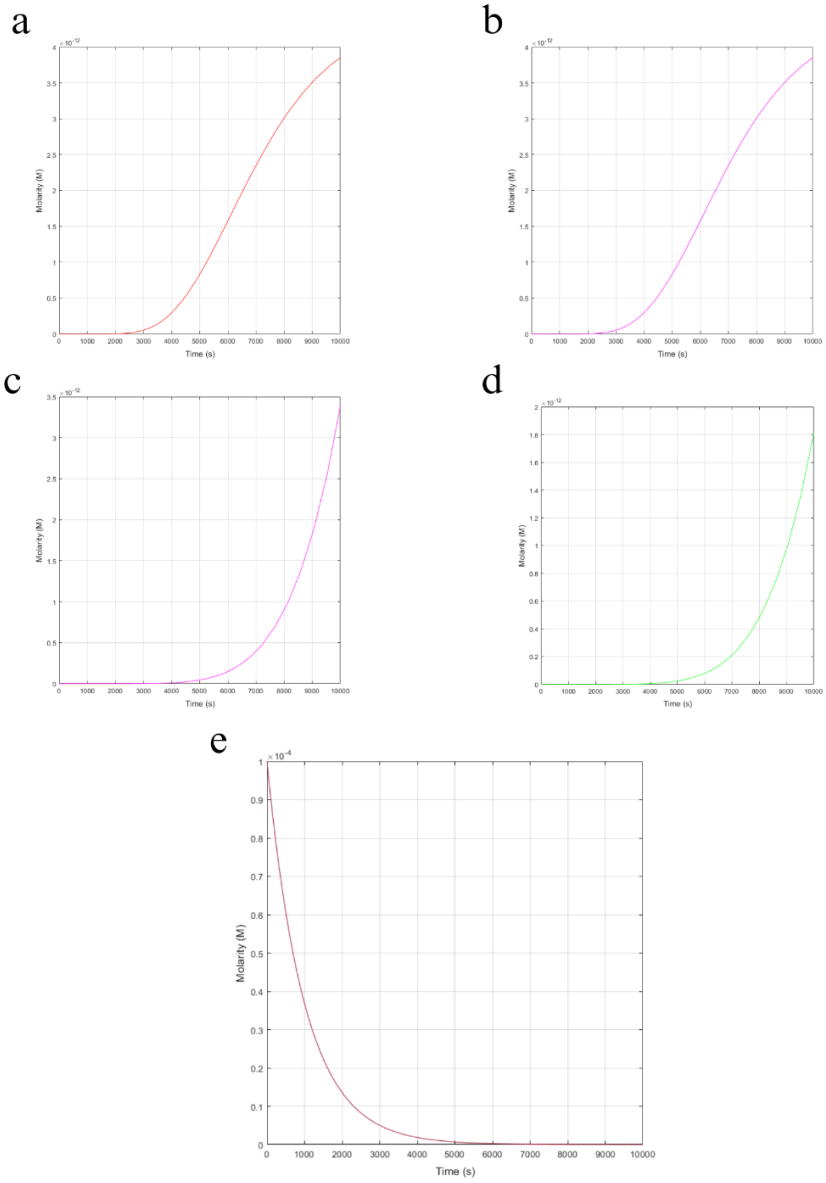

Figure 4: Molarity of TPA over time (a), molarity of EG over time (b), molarity of sbPETase over time (c), molarity of MHETase over time (d), and molarity of PET over time (e), respectively.

Given the rates of production of PETase and MHETase, the exponential increase in EG and TPA follows expectations. The order of magnitude suggests efficient PET breakdown at this step in the circuit, however the rates are still limited by the detection mechanism. Additionally, as EG is broken down further in the secondary degradation circuit, it would be expected that its concentrations would begin to decrease after plateauing. From the PET degradation, for the circuit to be viable, it would need to breakdown PET roughly 10^6 times faster than its natural degradation [25]. Given that that the half life of PET is 2500 years, our circuit is well above the threshold to be considered effectual [26].

Secondary PET Degradation (EG Degradation)

T7 also promotes the transcription of the enzyme cascade responsible for further degrading EG into its final, harmless byproducts (malate and CoA) as can be seen in *Figure 12*. The enzymes produced directly by this cascade are GR, GDH, and MS. Also transcribed are glycolate oxidase subunits D/E/F (GlcD, GlcE, and GlcF), which complex to form GO. As these enzymes are also produced through a T7 promoter, it is expected that the concentration-time graphs of GR, GDH, and MS will have similar exponential shapes. As can be seen in *Figures 5a* and *5c*, this expectation holds true in silico as the concentration responses of these enzymes display the expected exponential behaviour.

GO is expected to show exponential accumulation similar to GR, GDH, and MS, but with a slower initial rate as its formation depends on the availability of its component enzymes. The results from *Figure 5b* follow theory as its concentration increases exponentially, though more gradually than other enzymes.

With these degrative enzymes produced, EG will be broken down, in order, into glycolaldehyde, glycolate, glyoxylate, and finally into malate and CoA. The rate of production for each of these substances is proportional to concentration of both the substance by which it is immediately proceeded as well as the enzyme that causes this break down. We expect each byproduct of EG to model exponential rates of growth even faster than that of the substances by which they are produced. This theory is exactly what is observed in the results with each upstream product having a slower rate of concentration growth than its downstream products as can clearly be seen in *Figures 6a -6e.*

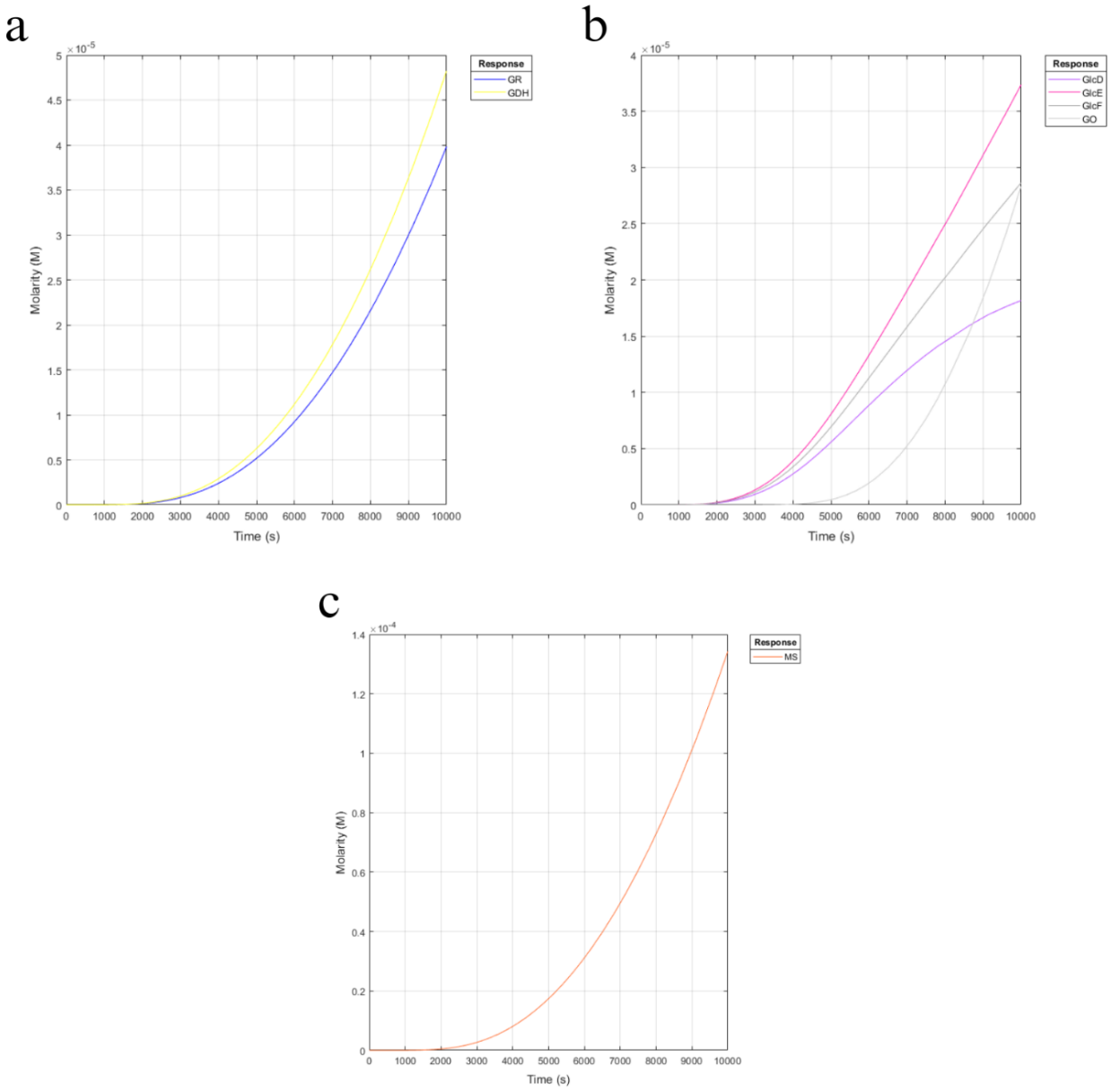

Figure 5: Molarity of GR and GDH over time (a), molarity of GO subunits and GO over time (b), molarity of MS over time (c).

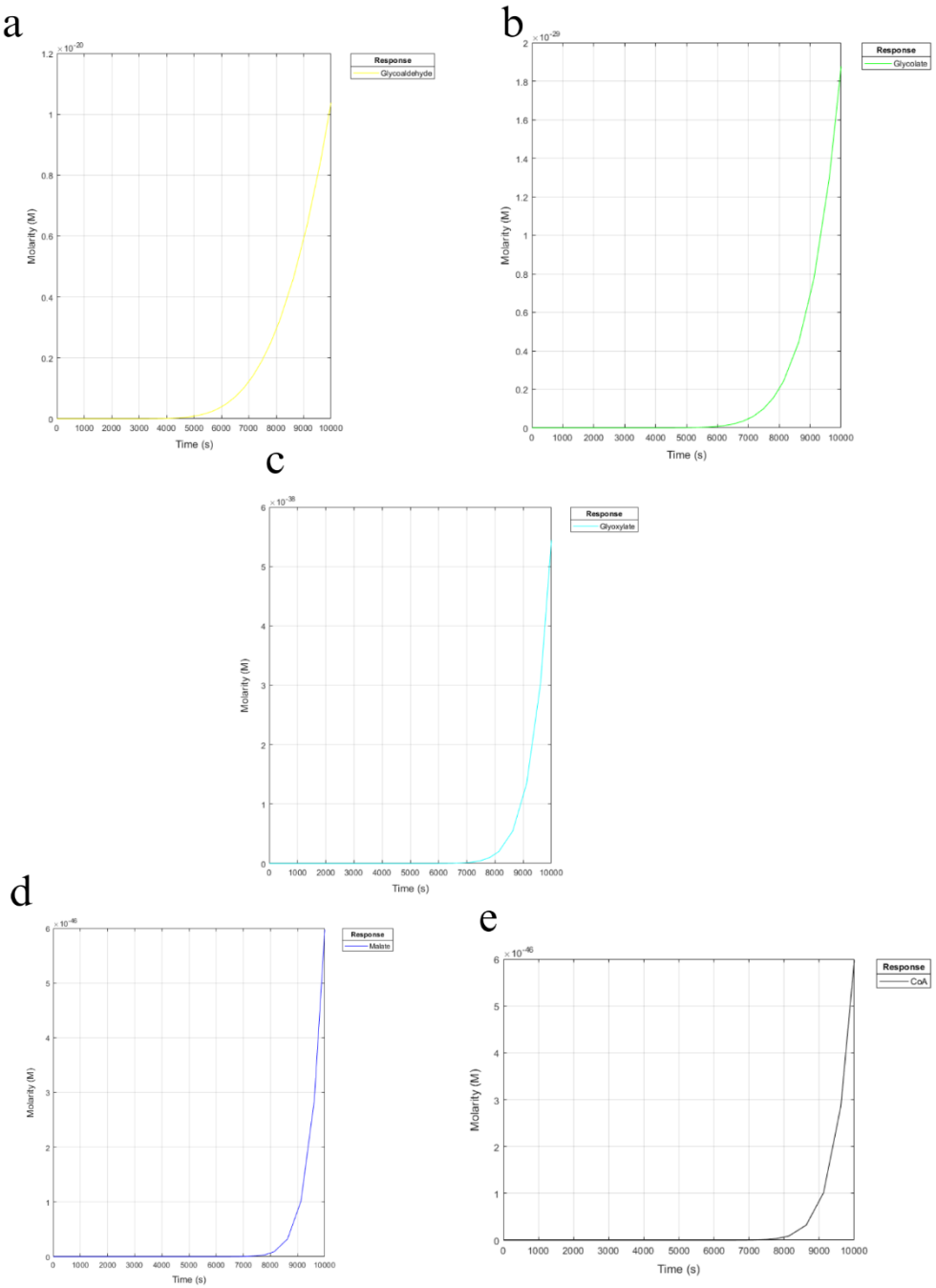

Figure 6: molarity of glycolaldehyde over time (a), molarity of glycolate over time (b), molarity of glyoxylate over time (c), molarity of malate over time (d), and molarity of CoA over time (e).

Limitations

There are a few key flaws and constraints of the circuit imposed on the Simbiology model. First, the complexation process of T7 in the model is based on the presence of two sub proteins, however in reality, the SupD-tRNA is not a product, rather an inhibitory tRNA that suppresses the mutation. Due to this constraint the observed behaviour of the SupD-tRNA, T7ptag protein, and T7 itself are all slightly unexpended results affecting the downstream production of key enzymes. In the degradation of PET to produce EG and TPA, it would be expected that EG would start to fall after plateauing, differing from TPA. This cannot be observed and is a result of large inefficiencies that occur downstream in the circuit in the breakdown of EG. Each sequential product in the cascade has a smaller magnitude of its concentration than the previous introducing significant bottlenecking. Thus, EG is broken down slowly and the circuit is limited by the inefficient enzyme production pathway. Despite the enzymes being produced at an acceptable rate, the overall pathway is unoptimized. The primary degradation of PET has appeared to be effaceable but the secondary degradation of EG is not.

Conclusion

The increasing accumulation of polyethylene terephthalate (PET) in the environment poses significant ecological and health risks. This study explored a synthetic biological solution, employing a genetic circuit in *Escherichia coli* to facilitate the enzymatic breakdown of PET. The engineered circuit was designed to be selectively activated in the presence of plastic derived compounds, ensuring precise enzyme expression only under environmentally relevant conditions. This targeted response enhances the overall efficiency of the degradation process.

The system successfully integrates functional modules, including a PET degradation module and an EG metabolism pathway. Simulation results highlighted the successful breakdown of PET and the conversion of EG into harmless metabolites, offering a significant improvement over existing degradation approaches that fail to address accumulation of toxic byproduct.

Despite promising outcomes, several limitations were identified. Key modeling assumptions may affect accuracy of the predicted behaviour. Also, the reliance on specific biomarkers limits the circuit's applicability across all PET containing products. Moreover, the accumulation of intermediate substrate and the dependence of downstream modules on the performance of upstream enzymes create metabolic bottlenecks that could hinder sustained activity.

To overcome these challenges, future iterations are required to develop more efficient strategies for biodegradation of PET. These may include the optimization of enzyme expression timing and ratios, the integration of alternative or synthetic promoters for improved control, and the development of feedback mechanisms to dynamically regulate metabolic flux.

Ultimately, the findings of this work demonstrate the potential of synthetic biology to address aggravating environmental issues. Through the design of biological systems, synthetic biology provides a powerful approach to combating plastic pollution and creating sustainable solutions for waste management.

Appendices

Tables and Parts

Table 1: Biological Parts of the Designed Circuit

Parts Code	Parts Name	Type	Function	References
BBa_K808000	araC-Pbad - Arabinose inducible promoter	promoter	Promoter that activates in the presence of Arabinose	[27]
BBa_K4164003	Retinoid X receptor-alpha(RXRα)	CDS	Produces RXR-alpha gene	[28]
BBa_K100009	Peroxisome Proliferator-activated receptor alpha	CDS	Produces PPAR-alpha gene	[29]
BBa_K1020001	alkM	promoter	Activates gene expression in the presence of alkanes	[30]
BBa_I719005	T7	promoter	Induces gene expression under the control of T7 RNA polymerase	[31]
BBa_K228001	SupD-tRNA	CDS	Suppresses amber mutation in T7ptag to allow transcription of T7 RNA polymerase	[32]
BBa_K228000	T7ptag (T7 polymerase with amber mutation)	CDS	Produces mRNA until SupD-tRNA represses amber codon to allow translation into T7 RNA polymerase	[33]
BBa_K4290022	SbPETase	CDS	Break down PET into smaller monomers	[34]
BBa_K3997001	MHETase	CDS	Converts MHET into TPA and EG	[35]
K936023	Glycolaldehyde Reductase (aerobic)	CDS	Convert EG into glycolaldehyde	[36]
K936011	Glycolaldehyde dehydrogenase	CDS	Coverts glycolaldehyde into glycolate	[37]
K2716200	Glycolate Oxidase Subunit D	CDS	Subunits form glycolate oxidase to convert glycolate into glyoxylate	[38]
K2716201	Glycolate Oxidase Subunit E	CDS		[39]
K2716202	Glycolate oxidase Subunit F	CDS		[40]

K1119003	aceB	CDS	Converts glyoxylate into malate for biomass growth	[41]
BBa_B0034	RBS (Elowitz 1999)	RBS	Ribosome binding site for translation initiation	[42]
BBa_K731721	T7 Terminator	Terminator	Stops transcription of the gene sequence	[43]
pSB1A3	High copy BioBrick assembly plasmid, pUC19-derived pMB1 ORI, ampicillin resistance	Plasmid Backbone	Vector for BioBricks to replicate synthetic circuit in *E. coli*	[44]

Table 2: Materials for Golden Gate Assembly

Material	Use	Supplier	References
BsaI-HF v2	Type IIS restriction enzyme for Golden Gate assembly	New England Biolabs	[45]
Plasmid Backbone (pSB3K3, pSB1A3, pSB4C5, pBBR1)	Plasmid backbone provides replication, selection, and scaffold for insert assembly	iGEM	[46]
T4 DNA Ligase	Ligase for joining DNA fragments with compatible overhangs	New England Biolabs	[47]
10x T4 DNA Ligase Buffer	Buffer for T4 DNA ligase activity	New England Biolabs	[48]
Nuclease-Free Water	Diluent for Golden Gate reactions	ThermoFisher	[49]

Table 3: Materials for PCR Reaction

Materials	Use	Supplier	References
Primers	Forward and reverse primers with BasI sites and overhangs	ThermoFisher	[50]
Phusion DNA Polymerase	High-fidelity PCR amplification	ThermoFisher	[51]
dNTPS	Nucleotides for PCR amplification	ThermoFisher	[52]
5x Phusion Buffer	Buffer for Phusion DNA polymerase	ThermoFisher	[53]
Nuclease-Free water	Diluent for PCR reactions	ThermoFisher	[54]

Table 4: Materials for Gel Electrophoresis and Purification

Materials	Use	Supplier	References

Agarose	Gel matrix for electrophoresis	Fisher Scientific	[55]
TAE Buffer	Buffer for running agarose gels	ThermoFisher	[56]
DNA Gel Extraction Kit	Purification of DNA fragments from agarose gel	New England Biolabs	[57]
DNA Ladder	Size marker for gel electrophoresis	ThermoFisher	[58]
GelRed Nucleic Acid Gel Stain	DNA stain for visualizing bands on gels`	ThermoFisher	[59]
Loading Dye	Prepare gel electrophoresis samples for loading	ThermoFisher	[60]

Table 5: Materials for Electroporation

Materials	Use	Supplier	References
Electrocompetent LMG194 E. coli cells	Cells for transformation	Intact Genomics	[61]
Sterile SOC media	Enhances post-electroporation recovery	Teknova	[62]
LMG194 strain of competent *E. coli* cell	These are required during electroporation and heat shock transformation	Fisher Scientific	[63]

Supplemental Materials

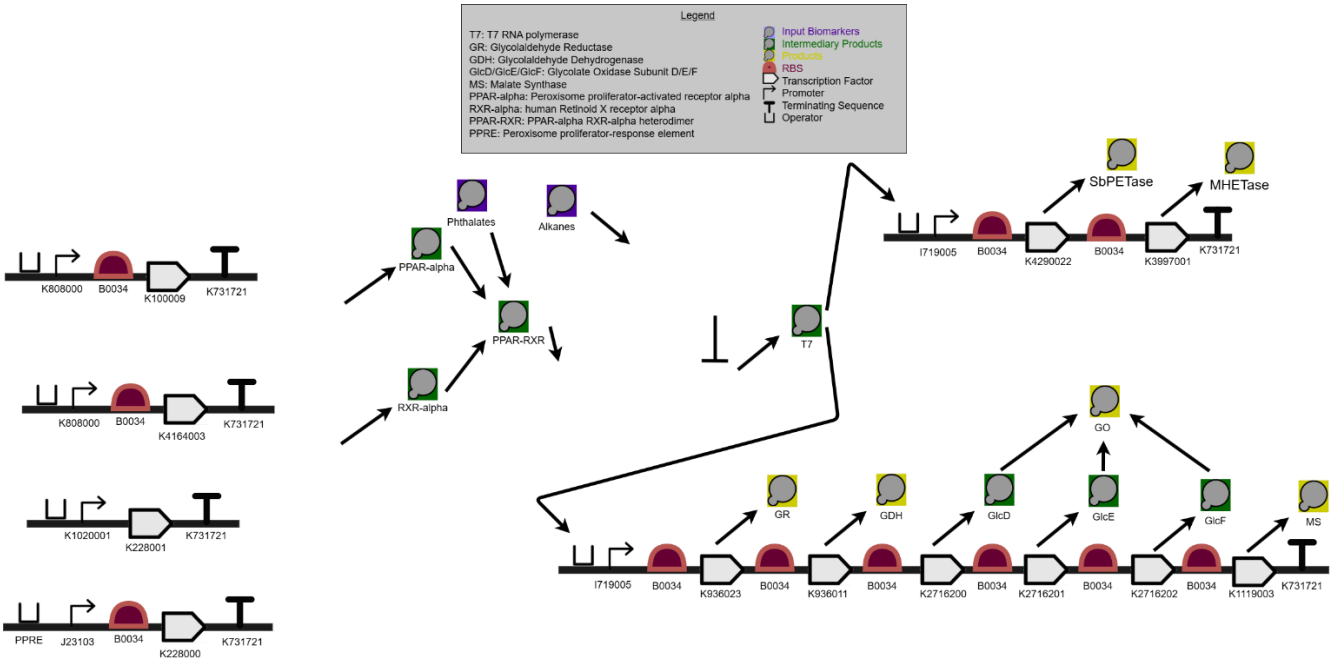

Figure 7: Complete SBOL of PET degradation circuit for reference.

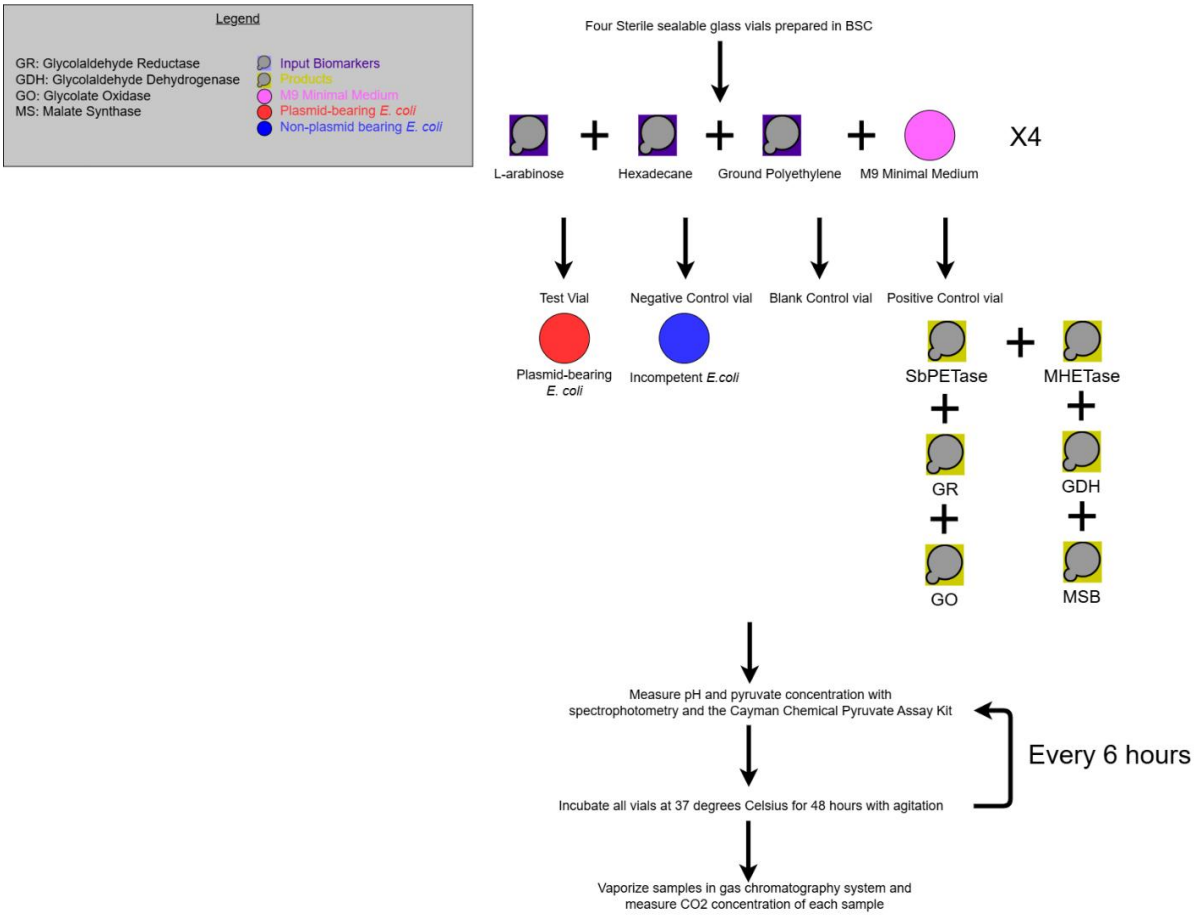

Figure 8: Experimental Schematic to Test the Efficacy of the Degradation Circuit.

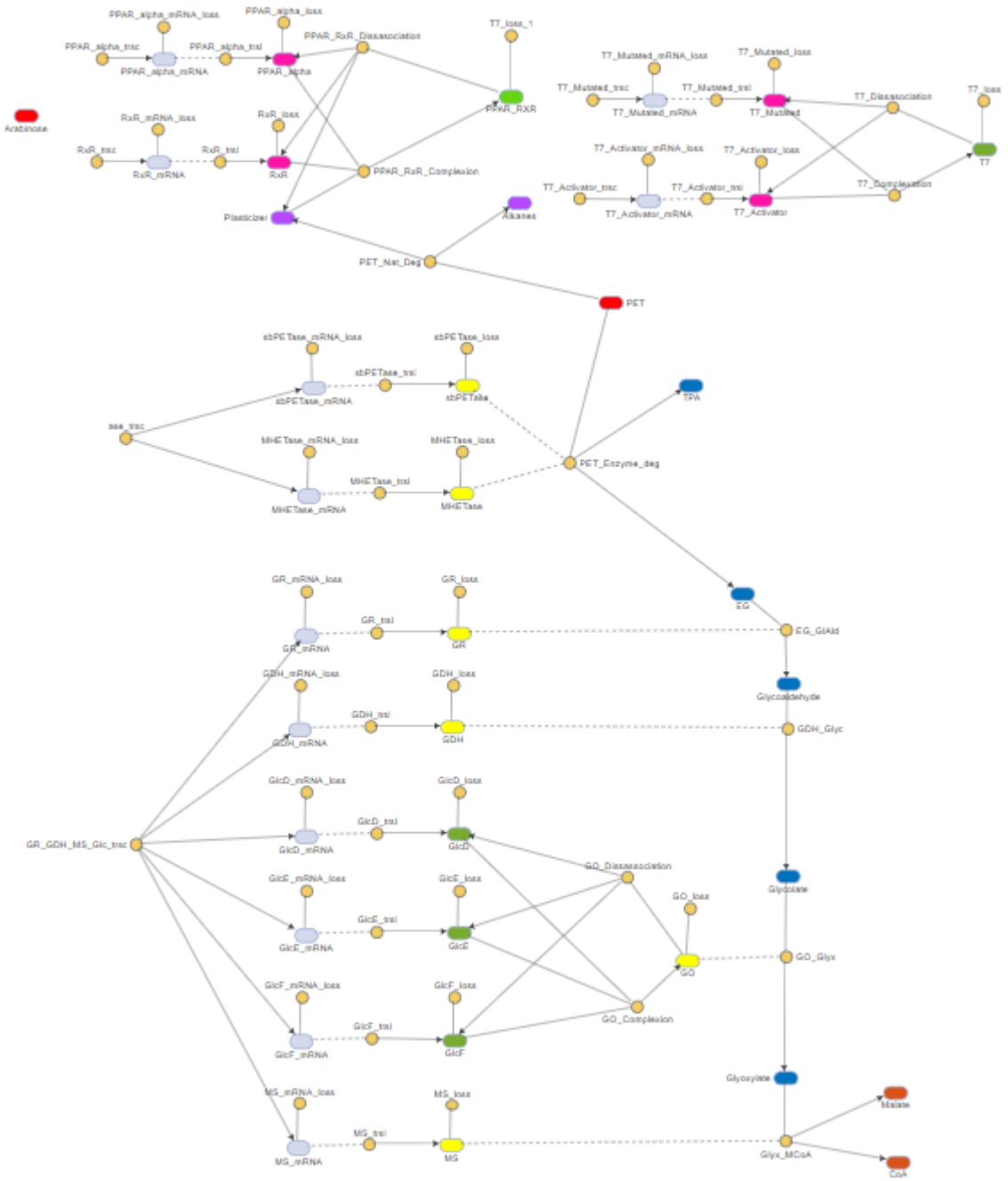

Figure 9: Complete MATLAB Simbiology model of the PET degradation circuit.

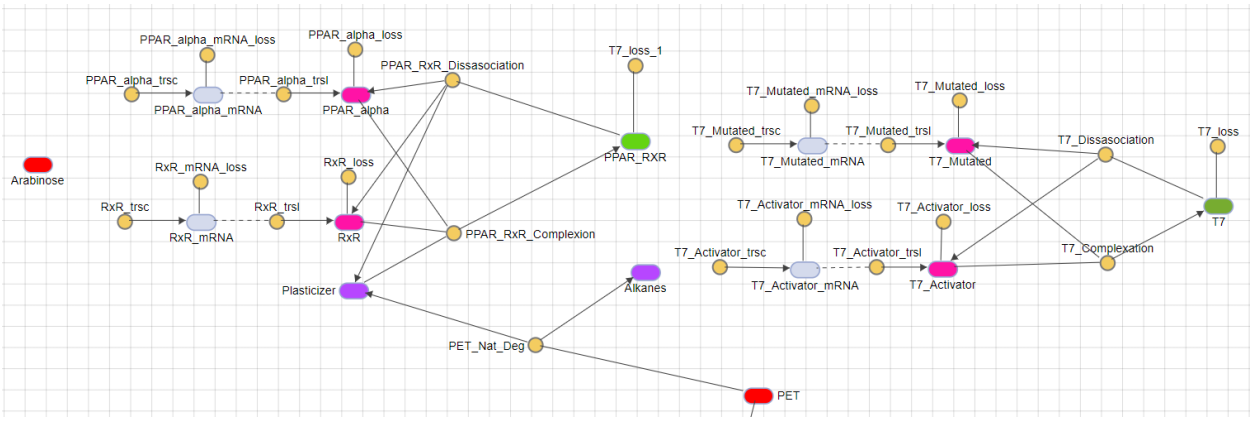

Figure 10: Magnified view of the T7 synthesis subcircuit.

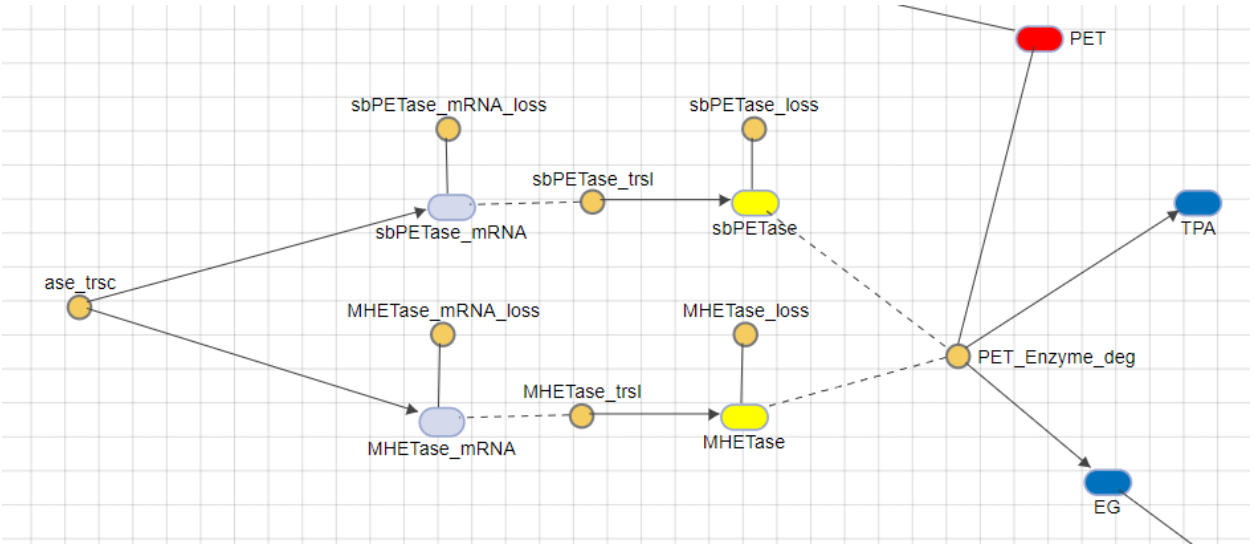

Figure 11: Magnified view of the PET enzymatic degradation subcircuit.

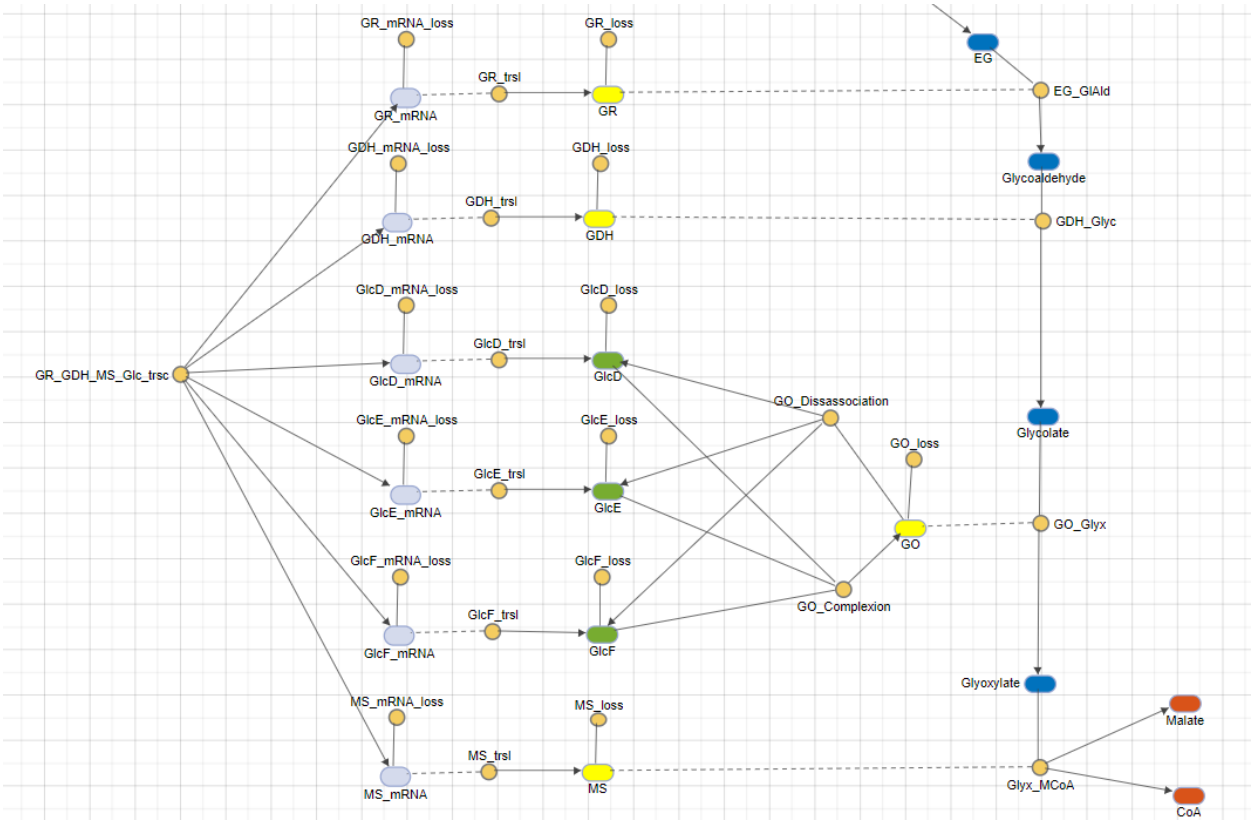

Figure 12: Magnified view of the EG enzymatic degradation cascade subcircuit.

References

[1] S. Shankar, S. Singh, A. Mishra, M. Sharma, and Shikha, "Microbial Degradation of Polyethylene: Recent Progress and Challenges," *Microorganisms for Sustainability*, vol. 10, pp. 245–262, 2019, doi: 10.1007/978-981-13-7462-3_12/TABLES/3.

[2] W. Xu *et al.*, "Evolution of the global polyethylene waste trade system," *Ecosystem Health and Sustainability*, vol. 6, no. 1, Dec. 2020, doi: 10.1080/20964129.2020.1756925/ASSET/925CE0A4-A448-4DCC-9F75-2E372358B435/ASSETS/GRAPHIC/TEHS_A_1756925_F0006_OC.JPG.

[3] V. Dhaka *et al.*, "Occurrence, toxicity and remediation of polyethylene terephthalate plastics. A review," *Environmental Chemistry Letters*, vol. 20, no. 3, pp. 1777–1800, Jan. 2022, doi: https://doi.org/10.1007/s10311-021-01384-8.

[4] M. Wang, Y. Wu, G. Li, Y. Xiong, Y. Zhang, and M. Zhang, "The hidden threat: Unraveling the impact of microplastics on reproductive health," *Science of The Total Environment*, vol. 935, p. 173177, Jul. 2024, doi: https://doi.org/10.1016/j.scitotenv.2024.173177.

[5] N. F. S. Khairul Anuar *et al.*, "An Overview into Polyethylene Terephthalate (PET) Hydrolases and Efforts in Tailoring Enzymes for Improved Plastic Degradation," *International Journal of Molecular Sciences*, vol. 23, no. 20, p. 12644, Jan. 2022, doi: https://doi.org/10.3390/ijms232012644.

[6] A. Walter, L. Sopracolle, M. Mutschlechner, M. Spruck, and C. Griesbeck, "Biodegradation of different PET variants from food containers by Ideonella sakaiensis," *Archives of Microbiology*, vol. 204, no. 12, Nov. 2022, doi: https://doi.org/10.1007/s00203-022-03306-w.

[7] D. Martín-González, C. de la Fuente Tagarro, A. De Lucas, S. Bordel, and F. Santos-Beneit, "Genetic Modifications in Bacteria for the Degradation of Synthetic Polymers: A Review," *International Journal of Molecular Sciences*, vol. 25, no. 10, p. 5536, Jan. 2024, doi: https://doi.org/10.3390/ijms25105536.

[8] New England Biolabs, "Golden Gate Assembly Protocol for using NEB Golden Gate Assembly Mix (E1601)," 2018. [Online]. Available: https://www.neb.com/en-us/protocols/2018/10/02/golden-gate-assembly-protocol-for-using-neb-golden-gate-assembly-mix-e1601

[9] New England Biolabs, "BsaI-HFv2," [Online]. Available: https://www.neb.com/products/r3733-bsai-hfv2

[10] "Plasmid backbones/Assembly - parts.igem.org," *Igem.org*, 2025. https://parts.igem.org/Plasmid_backbones/Assembly (accessed Apr. 09, 2025).

[11] New England Biolabs, "Q5 High-Fidelity DNA Polymerase," [Online]. Available: https://www.neb.com/products/q5-high-fidelity-dna-polymerase

[12] Y. Soma *et al.*, “Trace impurities in sodium phosphate influences the physiological activity of Escherichia coli in M9 minimal medium,” *Scientific Reports*, vol. 13, no. 1, Oct. 2023, doi: https://doi.org/10.1038/s41598-023-44526-4.

[13] “Part:BBa K808000 - parts.igem.org,” *parts.igem.org*. https://parts.igem.org/Part:BBa_K808000

[14] P. Morgado, J. Barras, P. Duarte, and E. J. M. Filipe, “Solubility of water in n-alkanes: New experimental measurements and molecular dynamics simulations,” *Fluid Phase Equilibria*, vol. 503, p. 112322, Jan. 2020, doi: https://doi.org/10.1016/j.fluid.2019.112322.

[15] P. Morgado, J. Barras, P. Duarte, and E. J. M. Filipe, “Solubility of water in n-alkanes: New experimental measurements and molecular dynamics simulations,” *Fluid Phase Equilibria*, vol. 503, p. 112322, Jan. 2020, doi: https://doi.org/10.1016/j.fluid.2019.112322.

[16] P. Bernard, P. Stelmachowski, P. Broś, W. Makowski, and A. Kotarba, “Demonstration of the Influence of Specific Surface Area on Reaction Rate in Heterogeneous Catalysis,” *Journal of Chemical Education*, vol. 98, no. 3, pp. 935–940, Jan. 2021, doi: https://doi.org/10.1021/acs.jchemed.0c01101.

[17] R. H. Kruse, W. H. Puckett, and J. H. Richardson, “Biological safety cabinetry.,” *Clinical Microbiology Reviews*, vol. 4, no. 2, pp. 207–241, Apr. 1991, doi: https://doi.org/10.1128/cmr.4.2.207.

[18] N. Mohanan, Z. Montazer, P. K. Sharma, and D. B. Levin, “Microbial and Enzymatic Degradation of Synthetic Plastics,” *Frontiers in Microbiology*, vol. 11, no. 1664–302X, Nov. 2020, doi: https://doi.org/10.3389/fmicb.2020.580709.

[19] J. Barron, C. Ashton, and L. Geary, “The Effects of Temperature on PH Measurement A REAGECON TECHNICAL PAPER.” Available: https://knowledge.reagecon.com/wp-content/uploads/2019/12/The-Effects-of-Temperature-on-PH-Measurement.pdf?utm_source=chatgpt.com

[20] “Pyruvate Assay Kit.” Accessed: Mar. 03, 2025. [Online]. Available: https://cdn.caymanchem.com/cdn/insert/700470.pdf

[21] R. Scaffaro and L. Botta, “Degradation Behavior of Nanocomposite Polymer Blends,” *Elsevier eBooks*, pp. 423–447, Dec. 2013, doi: https://doi.org/10.1016/b978-1-4557-3159-6.00012-2.

[22] P. D. Vaidya and E. Y. Kenig, “Gas–Liquid Reaction Kinetics: A review of Determination Methods,” *Chemical Engineering Communications*, vol. 194, no. 12, pp. 1543–1565, Aug. 2007. doi:10.1080/00986440701518314

[23] “Team:PennState/smartfold/overview - 2008.igem.org,” *Igem.org*, 2025. https://2008.igem.org/Team:PennState/smartfold/overview (accessed Apr. 08, 2025).

[24] S. Yoshida, K. Hiraga, I. Taniguchi, and K. Oda, “Ideonella sakaiensis, PETase, and MHETase: From identification of microbial PET degradation to enzyme

characterization," *Methods in Enzymology*, vol. 648, pp. 187–205, 2021, doi: https://doi.org/10.1016/bs.mie.2020.12.007.

[25] A. Yip, O. D. McArthur, K. C. Ho, M. G. Aucoin, and B. P. Ingalls, "Degradation of polyethylene terephthalate (PET) plastics by wastewater bacteria engineered via conjugation," *Microbial Biotechnology*, vol. 17, no. 9, Sep. 2024, doi: https://doi.org/10.1111/1751-7915.70015.

[26] A. Chamas *et al.*, "Degradation rates of plastics in the environment," *ACS Sustainable Chemistry & Engineering*, vol. 8, no. 9, pp. 3494–3511, Feb. 2020, doi: https://doi.org/10.1021/acssuschemeng.9b06635.

[27] "Part:BBa K808000 - parts.igem.org," *parts.igem.org*. https://parts.igem.org/Part:BBa_K808000

[28] "Part:BBa K4164003 - parts.igem.org," *Igem.org*, 2022. https://parts.igem.org/Part:BBa_K4164003 (accessed Apr. 09, 2025).

[29] "Part:BBa K100009 - parts.igem.org," *Igem.org*, 2025. https://parts.igem.org/Part:BBa_K100009 (accessed Apr. 09, 2025).

[30] P. D. Vaidya and E. Y. Kenig, "Gas–Liquid Reaction Kinetics: A review of Determination Methods," Chemical Engineering Communications, vol. 194, no. 12, pp. 1543–1565, Aug. 2007. doi:10.1080/00986440701518314

[31] "Part:BBa K206000 - parts.igem.org," *Igem.org*, 2019. https://parts.igem.org/Part:BBa_K206000 (accessed Mar. 03, 2025).

[32] "Part:BBa I719005 - parts.igem.org," *Igem.org*, 2018. https://parts.igem.org/Part:BBa_I719005

[33] "Part:BBa K228001:Design - parts.igem.org," *Igem.org*, 2025. https://parts.igem.org/Part:BBa_K228001:Design

[34] "Part:BBa K228000 - parts.igem.org," *parts.igem.org*. https://parts.igem.org/Part:BBa_K228000

[35] "Part:BBa K4290022 - parts.igem.org," *Igem.org*, 2022. https://parts.igem.org/Part:BBa_K4290022 (accessed Mar. 03, 2025).

[36] "Part:BBa K3997001 - parts.igem.org," *Igem.org*, 2021. https://parts.igem.org/Part:BBa_K3997001 (accessed Mar. 03, 2025).

[37] "Part:BBa K936023 - parts.igem.org," *Igem.org*, 2025. https://parts.igem.org/Part:BBa_K936023 (accessed Mar. 03, 2025).

[38] "Part:BBa K936011 - parts.igem.org," *Igem.org*, 2025. https://parts.igem.org/Part:BBa_K936011 (accessed Mar. 03, 2025).

[39] "Part:BBa K2716200 - parts.igem.org," *Igem.org*, 2018. https://parts.igem.org/Part:BBa_K2716200 (accessed Mar. 03, 2025).

[40] "Part:BBa K2716201 - parts.igem.org," *Igem.org*, 2018. https://parts.igem.org/Part:BBa_K2716201 (accessed Mar. 03, 2025).

[41] "Part:BBa K2716202 - parts.igem.org," *Igem.org*, 2018. https://parts.igem.org/Part:BBa_K2716202 (accessed Mar. 03, 2025).

[42] “Part:BBa K1119003:Design - parts.igem.org,” *Igem.org*, 2025. https://parts.igem.org/Part:BBa_K1119003:Design (accessed Mar. 03, 2025).
[43] “Part:BBa B0034 - parts.igem.org,” *parts.igem.org*. https://parts.igem.org/Part:BBa_B0034
[44] “Part:BBa K731721 - parts.igem.org,” *Igem.org*, 2019. https://parts.igem.org/Part:BBa_K731721 (accessed Mar. 03, 2025).
[45] “Part:pSB1A3 - parts.igem.org,” *Igem.org*, 2025. https://parts.igem.org/wiki/index.php?title=Part%3ApSB1A3 (accessed Mar. 03, 2025).
[46] iGEM Registry of Standard Biological Parts, "Plasmid backbones/Assembly," [Online]. Available: https://parts.igem.org/Plasmid_backbones/Assembly
[47] New England Biolabs, *Neb.com*, 2020. https://www.neb.com/en/products/r3733-bsai-hf-v2?srsltid=AfmBOorLhxOPKTyfMialoEgUil1B6Y1kTWM8KYpapv2bMk9fRIAyLI2d (accessed Mar. 03, 2025).
[48] New England Biolabs, *Neb.com*, 2019. https://www.neb.com/en/products/m0202-t4-dna-ligase?srsltid=AfmBOorS08MQG1GxD0H8t-D9k0UDr9H4gWAIOHV4qRnL0xqg94Kl7i-8 (accessed Mar. 03, 2025).
[49] “Addgene: Empty Backbones - Choosing Your Perfect Plasmid Backbone,” *Addgene.org*, 2025. https://www.addgene.org/collections/empty-backbones/?utm_source=chatgpt.com (accessed Mar. 03, 2025).
[50] “GeneArt Gene Synthesis | Thermo Fisher Scientific - US,” *Thermofisher.com*, 2024. https://www.thermofisher.com/ca/en/home/life-science/cloning/gene-synthesis/geneart-gene-synthesis.html?gclid=Cj0KCQiAoJC-BhCSARIsAPhdfShEAOP9PdoEwx2oTQpSUR5qaWlzXkmKzrUHXl7l64GclYT4CiaZ_z0aAqMrEALw_wcB&ef_id=Cj0KCQiAoJC-BhCSARIsAPhdfShEAOP9PdoEwx2oTQpSU (accessed Mar. 03, 2025).
[51] “Custom DNA Oligos | Thermo Fisher Scientific - US,” *Thermofisher.com*, 2024. https://www.thermofisher.com/ca/en/home/life-science/oligonucleotides-primers-probes-genes/custom-dna-oligos.html
[52] “Phusion DNA Polymerases & Master Mixes | Thermo Fisher Scientific - US,” *Thermofisher.com*, 2024. https://www.thermofisher.com/ca/en/home/brands/thermo-scientific/molecular-biology/thermo-scientific-pcr/high-fidelity-dna-polymerases-master-mixes-thermo-scientific.html?gclid=Cj0KCQiAoJC-BhCSARIsAPhdfShrteLx9nffCPH-UrdZC1xUX6_S3mHr0Fp22m9HLlIwsbu6Q8vc1 (accessed Mar. 03, 2025).
[53] Custom DNA Oligos | Thermo Fisher Scientific - US,” *Thermofisher.com*, 2024. https://www.thermofisher.com/ca/en/home/life-science/oligonucleotides-primers-probes-genes/custom-dna-oligos.html
[54] “Addgene: Empty Backbones - Choosing Your Perfect Plasmid Backbone,” *Addgene.org*, 2025. https://www.addgene.org/collections/empty-backbones/?utm_source=chatgpt.com (accessed Mar. 03, 2025).

[55] "dNTPs | Thermo Fisher Scientific," *Thermofisher.com*, 2015. https://www.thermofisher.com/search/browse/category/us/en/90217020 (accessed Mar. 03, 2025).

[56] "Agarose Electrophoresis Gels | Fisher Scientific," *Fishersci.ca*, 2024. https://www.fishersci.ca/ca/en/browse/90155046/agarose-electrophoresis-gels?page=1 (accessed Mar. 03, 2025).

[57] "TAE Buffer (Tris-acetate-EDTA) (50X)," *www.thermofisher.com*. https://www.thermofisher.com/order/catalog/product/B49

[58] "DNA and RNA Extraction and Analysis | Thermo Fisher Scientific - US," *Thermofisher.com*, 2024. https://www.thermofisher.com/ca/en/home/life-science/dna-rna-purification-analysis.html?gclid=Cj0KCQiAoJC-BhCSARIsAPhdfSgXOy25XRqJGP5yKMFFAexMCMMoWxRZYB-xMEjkVGMjen9juMbBp-EaAm6fEALw_wcB&ef_id=Cj0KCQiAoJC-BhCSARIsAPhdfSgXOy25XRqJGP5yKMFFAexMCMMoWxRZYB-xM (accessed Mar. 03, 2025).

[59] "DNA Ladders | Thermo Fisher Scientific - US," *Thermofisher.com*, 2024. https://www.thermofisher.com/ca/en/home/life-science/dna-rna-purification-analysis/nucleic-acid-gel-electrophoresis/dna-ladders.html (accessed Mar. 03, 2025).

[60] "Loading Dyes and Buffers – Thermo Scientific - US," *www.thermofisher.com*. https://www.thermofisher.com/ca/en/home/brands/thermo-scientific/molecular-biology/thermo-scientific-nucleic-acid-electrophoresis-purification/dna-electrophoresis-thermo-scientific/loading-dyes-buffers.html

[61] "SYBR Safe DNA Gel Stain | Thermo Fisher Scientific - US," *Thermofisher.com*, 2024. https://www.thermofisher.com/ca/en/home/life-science/dna-rna-purification-analysis/nucleic-acid-gel-electrophoresis/dna-stains/sybr-safe.html?gclid=Cj0KCQiA2oW-BhC2ARIsADSIAWrDAsmMNn4McAf7wuN_f06MKmA52gfAeHr4LfSsVsUG3tx_RviA_XoaAijPEALw_wcB&ef_id=Cj0KCQi (accessed Mar. 03, 2025).

[62] "Electrocompetent E. Coli Cells - Intact Genomics," *Intact Genomics*, Oct. 30, 2024. https://intactgenomics.com/electrocompetent-e-coli-cells/ (accessed Mar. 03, 2025).

[63] "ATCC Escherichia coli; LMG194," *Fishersci.com*, 2025. https://www.fishersci.com/shop/products/escherichia-coli-lmg194/502384105 (accessed Apr. 07, 2025).